Redox Biology 51 (2022) 102264

Contents lists available at ScienceDirect

Redox Biology

journal homepage: www.elsevier.com/locate/redox

Voltage Dependent Anion Channel 3 (VDAC3) protects mitochondria from oxidative stress

Simona Reina [a,d,*,1], Stefano Conti Nibali [a,1], Marianna Flora Tomasello [b], Andrea Magrì [c,d], Angela Messina [c,d], Vito De Pinto [a,d,e]

[a] Department of Biomedical and Biotechnological Sciences, University of Catania, Via S. Sofia 64, 95123, Catania, Italy
[b] Institute of Crystallography, National Council of Research, Catania Unit, Catania, 95126, Italy
[c] Department of Biological, Geological and Environmental Sciences, Section of Molecular Biology, University of Catania, Viale A. Doria 6, 95125, Catania, Italy
[d] We.MitoBiotech S.R.L., c.so Italia 172, 95129, Catania, Italy
[e] National Institute for Biostructures and Biosystems, Section of Catania, Rome, Italy

ARTICLE INFO

Keywords:
VDAC3
Cysteine
ROS
Mitochondria
Complex I
High-resolution respirometry

ABSTRACT

Unraveling the role of VDAC3 within living cells is challenging and still requires a definitive answer. Unlike VDAC1 and VDAC2, the outer mitochondrial membrane porin 3 exhibits unique biophysical features that suggest unknown cellular functions. Electrophysiological studies on VDAC3 carrying selective cysteine mutations and mass spectrometry data about the redox state of such sulfur containing amino acids are consistent with a putative involvement of isoform 3 in mitochondrial ROS homeostasis. Here, we thoroughly examined this issue and provided for the first time direct evidence of the role of VDAC3 in cellular response to oxidative stress. Depletion of isoform 3 but not isoform 1 significantly exacerbated the cytotoxicity of redox cyclers such as menadione and paraquat, and respiratory complex I inhibitors like rotenone, promoting uncontrolled accumulation of mitochondrial free radicals. High-resolution respirometry of transiently transfected HAP1-ΔVDAC3 cells expressing the wild type or the cysteine-null mutant VDAC3 protein, unequivocally confirmed that VDAC3 cysteines are indispensable for protein ability to counteract ROS-induced oxidative stress.

1. Introduction

Mitochondria are a major source of reactive oxygen species (ROS) as well as a critical target of the harmful effects of oxidative stress [1–3]: because of this they are equipped with multiple defense mechanisms [4]. These range from antioxidants enzymes, able to directly quench radical species (i.e. superoxide dismutases (SODs), glutathione peroxidase (GSH-Px) and peroxiredoxin/thioredoxin (PRX/Trx) systems [5,6]) to complex pathways including mitophagy and mitochondrial unfolded protein response (mtURP) [7,8]. Mitochondria communicate their redox state to targets located in the cytosol and in the nucleus (retrograde redox signaling) via mechanisms that are not fully understood but mostly rely on the modulation of redox sensitive proteins such as protein kinases [9,10]. In 2016, the Voltage Dependent Anion Channel isoform 3 (VDAC3) was suggested as a putative sensor of mitochondrial ROS levels [11,12]. Hitherto, VDAC1 had been considered a key player in ROS-induced apoptosis [13] as the responsible for the translocation of superoxide anion from mitochondria to cytosol [14]. Located in the outer membrane of eukaryotes mitochondria, VDACs form large aqueous channels that mediate metabolites exchange across the organelle [15,16]. They also participate in a wide range of pathways thanks to the interaction with cytosolic enzymes and both pro-apoptotic and anti-apoptotic factors [17,18]. The three VDAC isoforms (VDAC1, VDAC2 and VDAC3) that exist in mammals are considered functionally distinct, despite showing a high sequence similarity [19]. VDAC1 and VDAC2 are mainly involved in the regulation of bioenergetic and of mitochondria-mediated apoptosis, and also, they feature well-established electrophysiological properties which have been thoroughly investigated in artificial membranes [20]. Knowledge about isoform 3 is limited and its biophysical characteristics are still debated. The group of Colombini first reported that VDAC3 rarely inserted into planar lipid membranes as fully open pores that did not exhibit typical voltage-dependent gating [21]. Subsequently, Checchetto et al. described very small and ungated channels upon VDAC3 reconstitution

* Corresponding author. Department of Biomedical and Biotechnological Sciences, University of Catania, Via S. Sofia 64, 95123 Catania, Italy.
E-mail address: simona.reina@unict.it (S. Reina).
[1] These authors equally contributed to the work.

https://doi.org/10.1016/j.redox.2022.102264
Received 17 January 2022; Received in revised form 3 February 2022; Accepted 8 February 2022
Available online 12 February 2022
2213-2317/© 2022 The Authors. Published by Elsevier B.V. This is an open access article under the CC BY-NC-ND license (http://creativecommons.org/licenses/by-nc-nd/4.0/).

under non-reducing conditions [22]. The addition of reductants to the refolding procedures [23] or pre-incubation with DTT before electrophysiological analysis [24] significantly increased the current through VDAC3 which behaves as canonical voltage-gated VDAC pores albeit with a much lower insertion rate than isoform 1 and 2. Swapping experiments had previously suggested the involvement of cysteine residues in VDAC3 pore-activity [25]: the replacement of the VDAC3 N-terminus, containing two cysteines, with the homologous sequence of VDAC1, which has none, allowed isoform 3 to completely rescue the porin-less yeast temperature-sensitive phenotype [25]. However, the proof about the key function of these residues in the gating modulation of VDAC3 channels came later in Refs. [26,27]. The diverse content in cysteines is, indeed, a distinctive feature of the three isoforms: e.g. in human, VDAC1 has two, VDAC2 has nine and VDAC3 has six cysteines [28,29]. According to mass spectrometry analysis [30,31], all of these residues follow an evolutionarily conserved redox modification pattern, being oxidated or reduced probably depending on their location with respect to cytosol or IMS. In particular, the observation that the whole cysteine content of the isoform 3 is never detected as totally oxidized suggests that specific residues may undergo continuous oxidation-reduction cycles and strengthens the idea that they might be regulated or regulate intracellular ROS levels. However, experimental evidence is still missing. Clues from literature support the idea that VDAC3 may function as a redox-sensing protein. To date, a comprehensive proteomic analysis listed stress sensors and redox-mediating enzymes among the cytosolic proteins associated with VDAC3 [32] and a redox DIGE proteomic study performed on rat heart mitochondria identified VDAC3 as a preferred target of mitochondrial ROS generated by the complex III [33]. Furthermore, in a VDAC3 knock out mice, Zou et al. associated the lack of this isoform with the increase of mitochondrial ROS following a high-salt diet [34]. In another work [35], the authors speculated that the substantial increase of VDAC3 expression in non-metastatic endometrial cancers may correlate with dyslipidemia, a metabolic risk factor associated with the development of this type of tumor. Dyslipidemia could stimulate VDAC3 up-regulation through fatty acids and amine synthesis pathways responsible for ROS production within mitochondria. Very recently, VDAC3 was identified as severely oxidized in HEK293T and HeLa cells exposed to a photosensitizer compound that substantially increases mitochondria-specific oxidative stress [36].

In this work, near-haploid human HAP1 cells devoid of VDAC3 (HAP1-ΔVDAC3) were compared to VDAC1 knock out (HAP1-ΔVDAC1) and parental cell lines to test VDAC3 contribution in oxidative stress response. Along with a greater basal ROS production and a remarkable increase in the expression of the main antioxidant and detoxifying enzymes, the absence of VDAC3 considerably worsened cell resistance against mitochondrial ROS inducers. As confirmation, transfection of HAP1-ΔVDAC3 cell line with a cysteine-null (C0A) VDAC3 showed that cysteines are essential for the cell oxidative homeostasis. We here provide compelling evidence of the involvement of VDAC3 in mitochondrial redox-regulatory networks.

2. Results

2.1. VDAC3 knock out down-regulates mitochondrial biogenesis

HAP1 are a near-haploid cell line, of human leukemia origin, harboring a single copy of each chromosome, except for a disomic fragment of chromosome 15. Haploidy renders these cells a powerful tool for functional studies as genome editing ensures the full knock out of the target gene. In this work, HAP1 cells, devoid of VDAC1 or VDAC3, were exploited to analyze the contribution of isoform 3 in mitochondrial ROS metabolism and signaling. To this aim, we initially performed a phenotypic and molecular characterization of the novel cell lines. As shown in Supp. Fig. 1A, B and C, no appreciable differences were observed in morphology, proliferation (at least within the first 72 h) and survival rate among HAP1-ΔVDAC1, HAP1-ΔVDAC3 and parental cells. However, the quantification of both mRNA and protein levels demonstrated a significant dysregulation in the expression profiles of the other two isoforms in the absence of VDAC3: compared to the parental cell line, HAP1-ΔVDAC3 displayed an approximate 50% decrease and a concomitant approximate 70% increase of VDAC1 and VDAC2 proteins, respectively (Fig. 1A and B). VDAC1 knock out, conversely, did not considerably alter the expression levels of VDAC2 and VDAC3 (Fig. 1A and B). As changes in VDAC function/expression have been related to mitochondrial biogenesis dysfunction [37], the effects of VDAC1 and VDAC3 depletion on mitochondrial content were assessed by investigating the PGC-1α (peroxisome proliferator-activated receptor *gamma* coactivator 1a) signaling cascade. PGC-1α controls mitochondrial respiration and biogenesis by coactivating numerous transcription factors, including the nuclear respiratory factors NRF-1. PGC-1α also indirectly regulates the mtDNA transcription by modulating the expression of the mitochondrial transcription factor A (TFAM), which is coactivated by NRF-1. As illustrated in Fig. 1C, the expression of all these genes is significantly reduced in both HAP1 K.O. cell lines, although the lack of VDAC3 is associated with the greatest variations (more than 50% reduction in mitochondrial biogenesis markers). However, mtDNA copy number quantification by determining the mtDNA/nDNA ratio and western blot analysis of Succinate Dehydrogenase Complex Flavoprotein Subunit A (SDHA) (Fig. 1D–E) demonstrated a similar effect of VDAC1 and VDAC3 knock out on mitochondrial deregulation. The significant fall in the mitochondrial mass of both K.O. cell lines was accompanied by a considerable hyperpolarization across their inner mitochondrial membranes (Fig. 1F, G and 1H), which was more pronounced (approximately 38%) in cells devoid of VDAC1 and could be related to ADP exhaustion [38].

2.2. VDAC3 depletion weakens cellular defenses against ROS and stimulates expression of antioxidant enzymes

Clues about the involvement of VDAC3 in ROS homeostasis have been reported elsewhere [32,34–36]. To examine whether or not the absence of VDAC3 can influence the intracellular redox state, we measured the relative abundance of three antioxidant enzymes. As shown in Fig. 2A, catalase, superoxide dismutase 1 (SOD1) and thioredoxin (TRX) were significantly overexpressed in HAP1-ΔVDAC3 compared to parental cell line (0.59 ± 0.15, 1.18 ± 0.10 and 1.10 ± 0.11-fold increase, respectively). HAP1-ΔVDAC1 also exhibited an increment in catalase and TRX expression (0.74 ± 0.13 and 0.58 ± 0.12-fold increase, respectively) with respect to control cells, whereas a reduction of SOD1 (0.30 ± 0.14-fold decrease) was observed, in agreement with [39]. Overall, the expression pattern of these major antioxidant enzymes demonstrates that cells devoid of VDAC3 experience a greater oxidative stress. MitoSOX-Based Flow Cytometry, which specifically detect mitochondrial superoxide, confirmed the highest basal level of mitochondrial ROS in HAP1-ΔVDAC3 cells with respect to the parental cell line and to cells lacking VDAC1 (Fig. 2B) [40–43]. Interestingly, both VDAC1 and VDAC3 depletion led to a diminished amount of cytosolic ROS with respect to control cells, as revealed by flow cytometry quantification with DCFH probe (Fig. 2C). These findings could be a consequence of the enhanced expression of antioxidant enzymes that quickly remove the excess of ROS from the cytosol or otherwise be explained by the minor permeability of superoxide across the outer membrane of VDAC1 and VDAC3 K.O. mitochondria.

2.3. Challenge with ROS producing drugs reveals the importance of VDAC3 in fighting oxidative stress

The impact of drugs that trigger mitochondrial superoxide accumulation (i.e. rotenone, menadione and paraquat) was evaluated in HAP1 cells devoid of VDAC1 or VDAC3. The results suggest that VDAC3 has a role in oxidative stress response. According to Fig. 3A, cell survival of

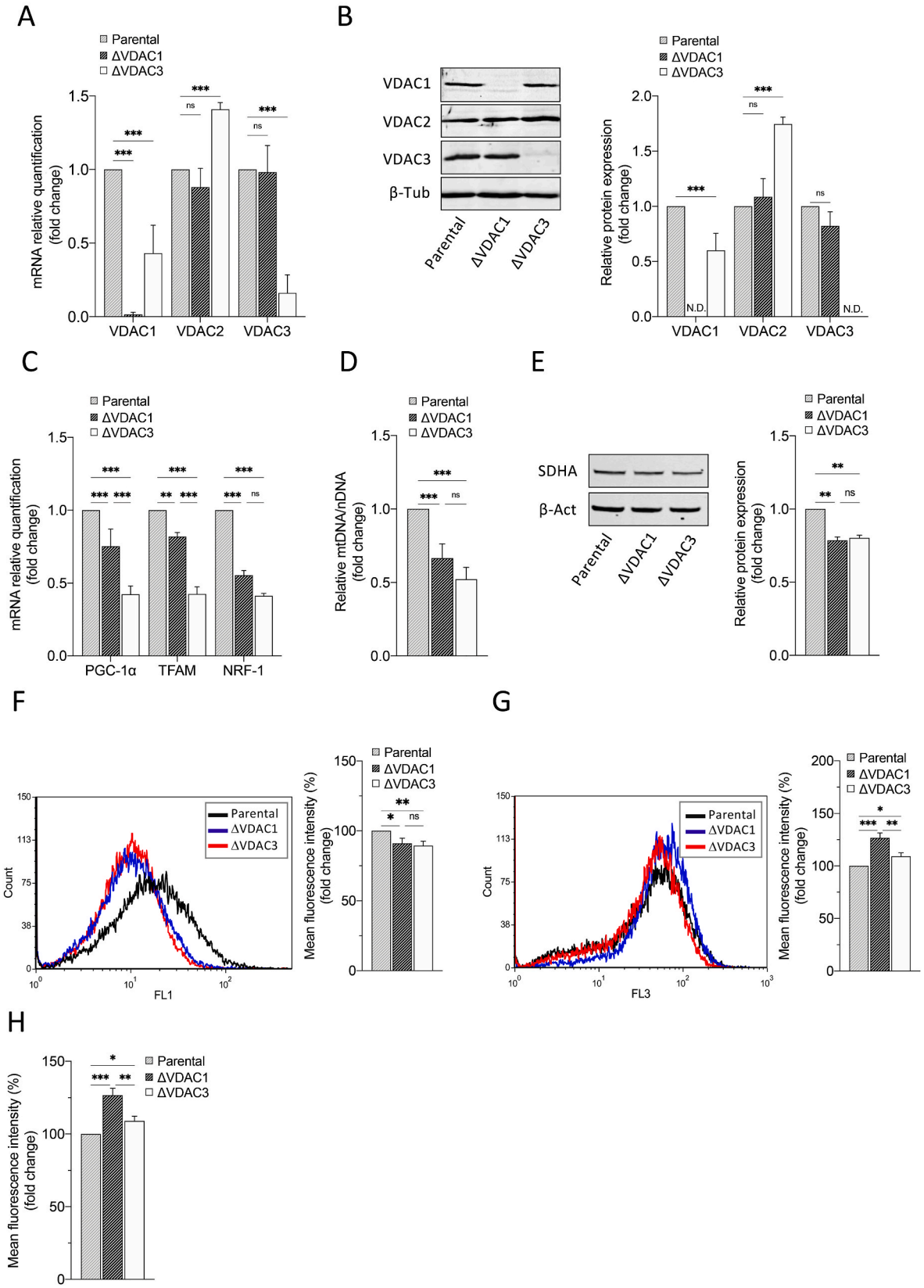

(caption on next page)

Fig. 1. Molecular characterization of HAP1 cell lines. A. Relative quantification of VDAC1, VDAC2 and VDAC3 mRNAs in HAP1-ΔVDAC1 and HAP1-ΔVDAC3. Data are normalized to the β-actin and expressed as means ± SEM (n = 3) and compared to HAP1 parental cells (equals one). B. Western blot illustration and relative quantification of VDAC1, VDAC2 and VDAC3 protein levels in HAP1-ΔVDAC1 and HAP1-ΔVDAC3. Data are normalized to the β-tubulin, expressed as means ± SEM (n = 3) and compared to HAP1 parental cells. C. Relative quantification of PGC-1α, NRF1 and TFAM (mitochondrial biogenesis markers) mRNAs in HAP1-ΔVDAC1 and HAP1-ΔVDAC3. Data are normalized to the β-actin and expressed as means ± SEM (n = 4) and compared to HAP1 parental cells. D. Quantification of mitochondrial DNA (mtDNA) in HAP1 cell lines devoid of VDAC1 or VDAC3. mtDNA amount was measured by Real-Time PCR of the mitochondrial gene COXII and normalized to the nuclear gene APP. Data are expressed as means ± SEM (n = 3) and compared to HAP1 parental cells. E. Quantification of mitochondrial content. Western blot illustration and relative quantification of mitochondrion-specific protein SDHA level in HAP1-ΔVDAC1 and HAP1-ΔVDAC3. Data are normalized to the β-Actin, expressed as means ± SEM (n = 3) and compared to HAP1 parental cells. F. Measurement of mitochondrial mass using MitoTracker Green. Representative fluorescence profiles of cells populations for the three cells lines. Histogram reports the average of fluorescence intensity measured by flow cytometry for the three HAP1 cell lines after proper gating of fluorescence. Gates were established based on negative and positive controls. Data are indicated as means ± SEM (n = 3) and compared to HAP1 parental cells. G. Detection of mitochondrial membrane potential by Mitotracker Red and measured by flow cytometry in each population of the three HAP1 cell lines. Histograms show the average fluorescence intensity measured for each gated cell population analyzed. Data are indicated as means ± SEM (n = 3) and compared to HAP1 parental cells. H. Quantification of mitochondrial membrane potential normalized for mitochondrial mass in HAP1 cell lines devoid of VDAC1 and VDAC3. Data are expressed as means ± SEM (n = 3) and compared to parental cell line. Data were analyzed with One-Way or Two-Way ANOVA; with *p < 0.05 **p < 0.01 and ***p < 0.001. (For interpretation of the references to colour in this figure legend, the reader is referred to the Web version of this article.)

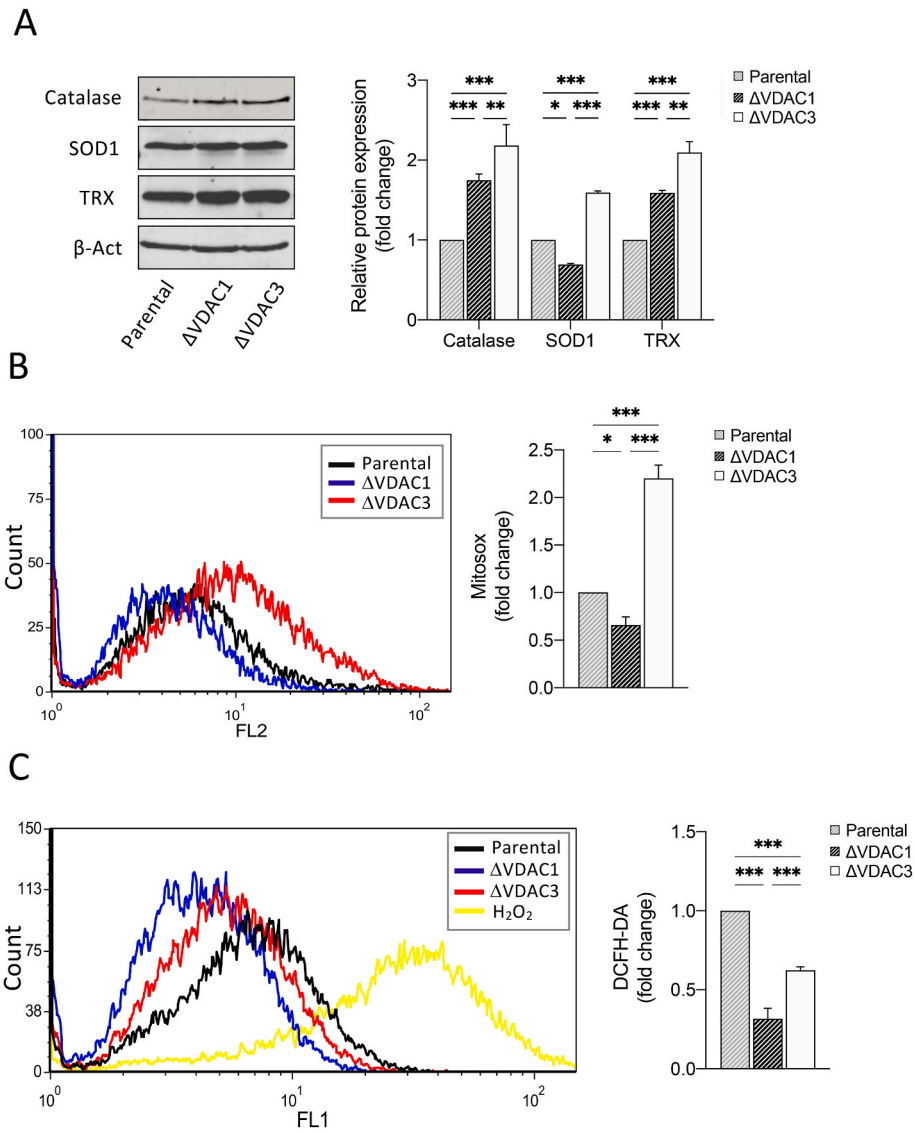

Fig. 2. Analysis of mitochondrial superoxide content and quantification of the expression levels of the main antioxidant enzymes in HAP1 cell lines. A. Representative immunoblot and relative protein quantification of antioxidant enzymes (Catalase, superoxide dismutase 1 (SOD1) and Thioredoxin (TRX)) in HAP1-ΔVDAC1 and HAP1-ΔVDAC3. Data are normalized to the β-actin, expressed as means ± SEM (n = 3) and compared to HAP1 parental cell line. B. Mitochondrial superoxide determination by MitoSOX red probe. Representative MitoSOX Red fluorescence profiles evaluated by flow cytometry in each population of HAP1 cell lines (left). Quantitative analysis of the mean fluorescence intensity MitoSOX Red in each population of HAP1 cell line. Results are expressed as the mean ± SD (n = 3) and compared to HAP1 parental cells (right). Results are expressed as the mean ± SD (n = 3) and compared to HAP1 parental cells. C. Intracellular ROS detected by DCFH-DA fluorescence measured by flow cytometer. Representative fluorescence profiles detected by flow cytometry for each cell line (left). Quantitative analysis of the average fluorescence intensity of DCFH-DA (%) in each gated population of HAP1 cell lines (right). Results are expressed as the mean ± SD (n = 3) and compared to HAP1 parental cell line. Data were analyzed with Two-Way ANOVA or One-Way ANOVA; with *p < 0.05 **p < 0.01 and ***p < 0.001. (For interpretation of the references to colour in this figure legend, the reader is referred to the Web version of this article.)

wild type HAP1 following paraquat, rotenone and menadione exposure, (MTT assay), ranged from 50 to 80%. VDAC3 knock out significantly reduced the percentage of viable cells by approx. 15% after paraquat and menadione treatments and by 40% upon rotenone administration. VDAC1 depletion did not affect cell sensitivity to rotenone and menadione, albeit, enhanced cell resistance to paraquat toxicity in accordance with Shimada et al. [44]. Relative quantification of protein levels in the parental cell line revealed that exposure to rotenone, menadione and paraquat mainly affected the expression profile of VDAC3 which is substantially up-regulated compared to VDAC1 and VDAC2 (Fig. 3B). To examine the endogenous mitochondrial superoxide production after a drug challenge in HAP1, control and K.O. cells were loaded with the

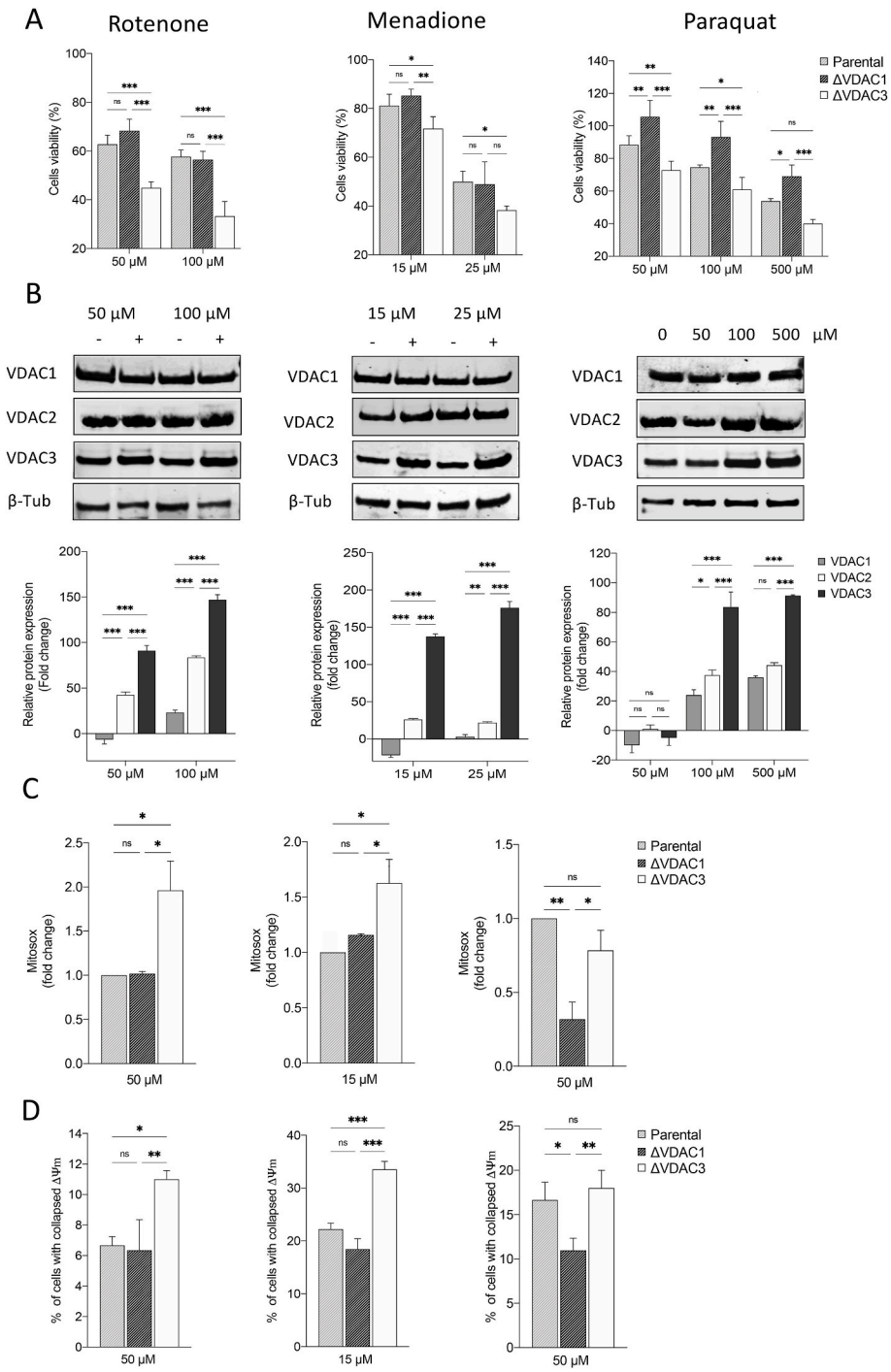

Fig. 3. Effect of mitochondrial ROS-inducers on cell viability, VDAC isoforms expression and mitochondria functionality. A. Cell viability of HAP1 cell lines treated with different concentrations of mitochondrial ROS-inducers (i.e., rotenone, menadione and paraquat). Data are indicated as the mean ± SE (n = 6) and expressed as the percentage ratio of the treated cells to the untreated ones. B. Relative quantification of VDAC1, VDAC2 and VDAC3 protein levels in HAP1 parental cells treated with increasing concentrations of rotenone, menadione and paraquat. All values are normalized to the β-tubulin endogenous control and expressed as means ± SEM (n = 3). C. Measurement of mitochondrial superoxide production via staining with MitoSOX Red after treatments with drugs. Data are expressed as mean ± SD (n = 3) and compared to HAP1 parental cell line. D. Mitochondrial membrane potential estimated by TMRM fluorescence measured with flow cytometry in HAP1 cell lines after drug administrations. Quantifications of percentage of cells with collapsed Δψm are indicated as means ± SEM (n = 3); mitochondrial membrane potential is normalized to mitochondrial mass value and expressed as the ratio of the treated cells to the untreated. Data were analyzed with Two-Way ANOVA or One-Way ANOVA; with *p < 0.05 **p < 0.01 and ***p < 0.001.

MitoSOX probe: following treatment with rotenone and menadione, flow cytometry measurements detected a significant increase (1.1 ± 0.10 and 0.65 ± 0.12-fold increase, respectively) in the amount of oxidized probe within HAP1-ΔVDAC3 cells with respect to the parental cell line (Fig. 3C). These same drugs did not remarkably enhance mitochondrial ROS production in VDAC1 K.O. cell line, where, on the contrary, a conspicuous reduction (0.68 ± 10 - fold decrease) in superoxide content was observed upon paraquat administration, compared to parental cell line (Fig. 3C). To this regard, unvaried ROS production in VDAC3-free cells compared to the wild-type cell line following treatment with paraquat may be explained by the down regulation of VDAC1, which mediates PQ toxicity. Consistent with the fact that oxidative stress caused by ROS can promote the rapid depolarization of the inner mitochondrial membrane potential, rotenone and menadione, but not paraquat, markedly increased the percentage of HAP1-ΔVDAC3 cells with collapsed ΔΨm (Fig. 3D). As expected, the mitochondrial membrane potential of parental and VDAC1 K.O cells was similarly affected by rotenone and menadione, whereas paraquat induced a considerable hyperpolarization of HAP1-ΔVDAC1 mitochondria compared to the other cell lines (Fig. 3D).

2.4. *Cysteine residues are responsible for the ability of VDAC3 to counteract mitochondrial ROS overload*

Previous reports led us to speculate that VDAC3 can modulate mitochondrial ROS content through the redox modifications of its

cysteine residues: most of them are indeed exposed towards the inter membrane space, an acidic and oxidative environment where ROS are released by Complex I [28]. To confirm this, HAP1-ΔVDAC3 cells were transiently transfected with plasmids encoding HA-tagged VDAC3 or VDAC3 C0A (i.e. a mutant where all cysteine residues were replaced with alanine residues), together with the mitochondrial-targeted Red Fluorescent Protein (mtDsRed) used as transfection reporter and as a mitochondrial marker. Before transfections, Mito Tracker Red DsRed staining allowed to portray the characteristic of mitochondrial network in parental and VDAC3 K.O. cells (Suppl. Fig. 2A). Flow cytometry and western blot confirmed the expression of the exogenous genes and revealed an approx. 70% transfection efficiency for both VDAC3 and VDAC3 C0A, which were also properly targeted to mitochondria (Fig. 4 A, B and Suppl. Fig. 2B). Strikingly, expression of VDAC3 induced nearly a 40% increase in HAP1-ΔVDAC3 cell survival after 24h exposure to 50 and 100 μM rotenone (Fig. 4C). Under the same experimental conditions, VDAC3 C0A did not considerably affect the susceptibility of VDAC3 knock out cells to the drug. These results are particularly impressive since neither VDAC3 nor VDAC3 C0A transfections altered mitochondrial content (Fig. 4D and E); furthermore, they did not stimulate a compensatory increase in VDAC1 protein level which could eventually disguise VDAC3 depletion (Suppl. Fig. 3). The boost in cell survival registered upon transfection with the wild type VDAC3 isoform is therefore unequivocally due to its cysteine residues that can counteract rotenone-induced mitochondrial injury. In support of these data, VDAC3 down-regulated catalase, thioredoxin and SOD1 expression more than the cysteine-null mutant, suggesting once again that restoring the wild-type protein expression is sufficient and necessary to reduce oxidative stress (Fig. 4F).

2.5. *VDAC3 preserves mitochondrial respiration upon oxidative stress conditions*

Rotenone is a powerful inhibitor of the mitochondrial electron transport system (ETS) complex I and exerts its toxicity by increasing mitochondrial ROS in the presence of NADH-linked substrates, through a mechanism not completely understood [45,46]. Given previous results, we queried whether VDAC3 could protect the mitochondrial respiration upon rotenone exposure. To this aim, High-Resolution Respirometry (HRR) was used to assay oxygen consumption of HAP1 cells.

Fig. 5A displays a representative respirometric curve of untreated parental HAP1 cells along with the specific protocol used herein. Briefly, oxygen consumption was first measured in intact cells, i.e., in the presence of endogenous substrates (ROUTINE state). Then, cells were permeabilized and the oxidative phosphorylation sustained by complex I was achieved in the presence of NADH-linked substrates (N-pathway, i.e. the contribution of complex I to the oxidative phosphorylation). Finally, the maximal electron transport (ET) capacity was obtained by the complete dissipation of the proton gradient through uncoupler titration.

In order to identify a sublethal rotenone dose, parental HAP1 cells were first exposed to increasing concentration of the toxin. In parallel, experiments were repeated using myxothiazol as a control. Myxothiazol blocks the ETS specifically acting on complex III [47] but without exerting any significant effect on ROS level [48,49]. As reported in Suppl. Fig. 4A–B, both drugs promoted a similarly significant decrease of parental HAP1 oxygen consumption in all the analyzed respiratory states in a dose-dependent manner starting from 100 nM, with the effect of rotenone being more pronounced than that of myxothiazol. On the other hand, no significant variation was observed at 10 nM rotenone. Additionally, this concentration did not affect cell viability (Suppl. Fig. 4C) nor in the case of rotenone neither upon myxothiazol treatment. Contrariwise, while the exposure of HAP1 cells to 10 nM rotenone correlated with an increase of about 58% in Mitosox signal in comparison to the untreated control, upon myxothiazol the Mitosox signal decreased (Suppl. Fig. 4D), suggesting a reduction of ROS production upon blockage of the ETS, in accordance with previous observations [50]. HRR experiments were also performed in HAP1-ΔVDAC3 cells transfected with constructs encoding VDAC3 or VDAC3 C0A, and exposed to the sublethal doses of rotenone and myxothiazol. While the transfections *per se* did not change respiration in any analyzed state (Suppl. Fig. 5), the absence of VDAC3 made HAP1 extremely sensitive to 10 nM rotenone: not only did the toxin halve cell viability (Fig. 5B) but significantly affected the respiration. As shown in Fig. 5C, VDAC3 knock out cells underwent a significant reduction of about 40% in the oxygen consumption during ROUTINE state, and of 65% and 70% in N-pathway and ET capacity, respectively. In contrast, absence of VDAC3 had no impact for cell viability or respiration of HAP1 (Fig. 5D–E) when cells are exposed to myxothiazol, since no significative variations were observed in all the conditions tested here. In any case, the re-introduction of VDAC3 with transient transfection almost nullified the harmful effect of rotenone, restoring cell survival and oxygen consumption in all the analyzed states (Fig. 5B–C). The expression of the *cys-null* mutant also improved both cell survival (Fig. 5B) and respiration (Fig. 5C) although the oxygen consumption levels never reached those of cells expressing VDAC3 WT. Again, no significative variations were observed upon VDAC3 WT or C0A mutant expression in VDAC3 knock out cells exposed to 10 nM myxothiazol (see Supplementary Table S1 for raw data).

Overall, these results indicate that VDAC3, and particularly the cysteine residues, is pivotal in maintaining mitochondrial functionality upon oxidative stress conditions.

3. Discussion

VDAC3 is the most recently discovered VDAC isoform [50]. Its existence raised questions about porin redundancy in the outer mitochondrial membrane. As for gram-negative bacteria, where many outer membrane porins absolve to specialized functions [51], mammalian VDAC isoforms accomplish distinct roles within the cell [52]. In particular, VDAC3 has recently been proposed to function as a sensor for the oxidation-reduction potential present in the mitochondrion [26,28]. To challenge this hypothesis, we deeply investigated the behavior of the human HAP1 cell lines devoid of VDAC1 or VDAC3 in response to ROS. Indeed, VDAC1 has been suggested to be involved in ROS homeostasis as well [41,53,54]: however, unlike VDAC3, isoform 1 would promote oxidative stress as speculated by Maldonado et al. [55] and demonstrated by Yang et al. [56]. The near haploid chromosomal status of HAP1 ensures the complete removal of the target gene: notwithstanding, in the particular case of VDAC, the remaining isoforms can potentially compensate for the knockout of a specific isoform and hence mask the effects of its depletion. For instance, in mouse embryonic stem (ES) cells, upon VDACs knock out a compensatory increase in VDAC1 expression was registered in VDAC2$^{-/-}$ and VDAC3$^{-/-}$ [56].

The preliminary characterization of HAP1-ΔVDAC1 and HAP1-ΔVDAC3 cells revealed no significant changes in the protein levels of VDAC2 and VDAC3 in HAP1-ΔVDAC1, whereas a simultaneous down-regulation of VDAC1 and up-regulation of VDAC2 was registered in HAP1-ΔVDAC3 cells. Interestingly, these data are in agreement with the positive association between VDAC1 and VDAC3 protein expression and the negative correlation of VDAC2 with VDAC1 detected in endometrial cancer cells [35]. Both knock out cell lines exhibited a considerable reduction in mitochondrial content with a concomitant increase in mitochondrial membrane potential. In other words, cells lacking VDAC1 or VDAC3 share a fewer number of mitochondria that, however, are more polarized. In accordance with our data, Magrì et al. previously reported that the absence of the endogenous yeast VDAC1 induces a metabolic rewiring through the down-regulation of mitochondria [37]. On the other hand, explaining the reasons for mitochondrial hyperpolarization upon VDACs knock out is arduous: one hypothesis is that it could be correlated to ADP depletion and loss of F_OF_1 ATPase activity,

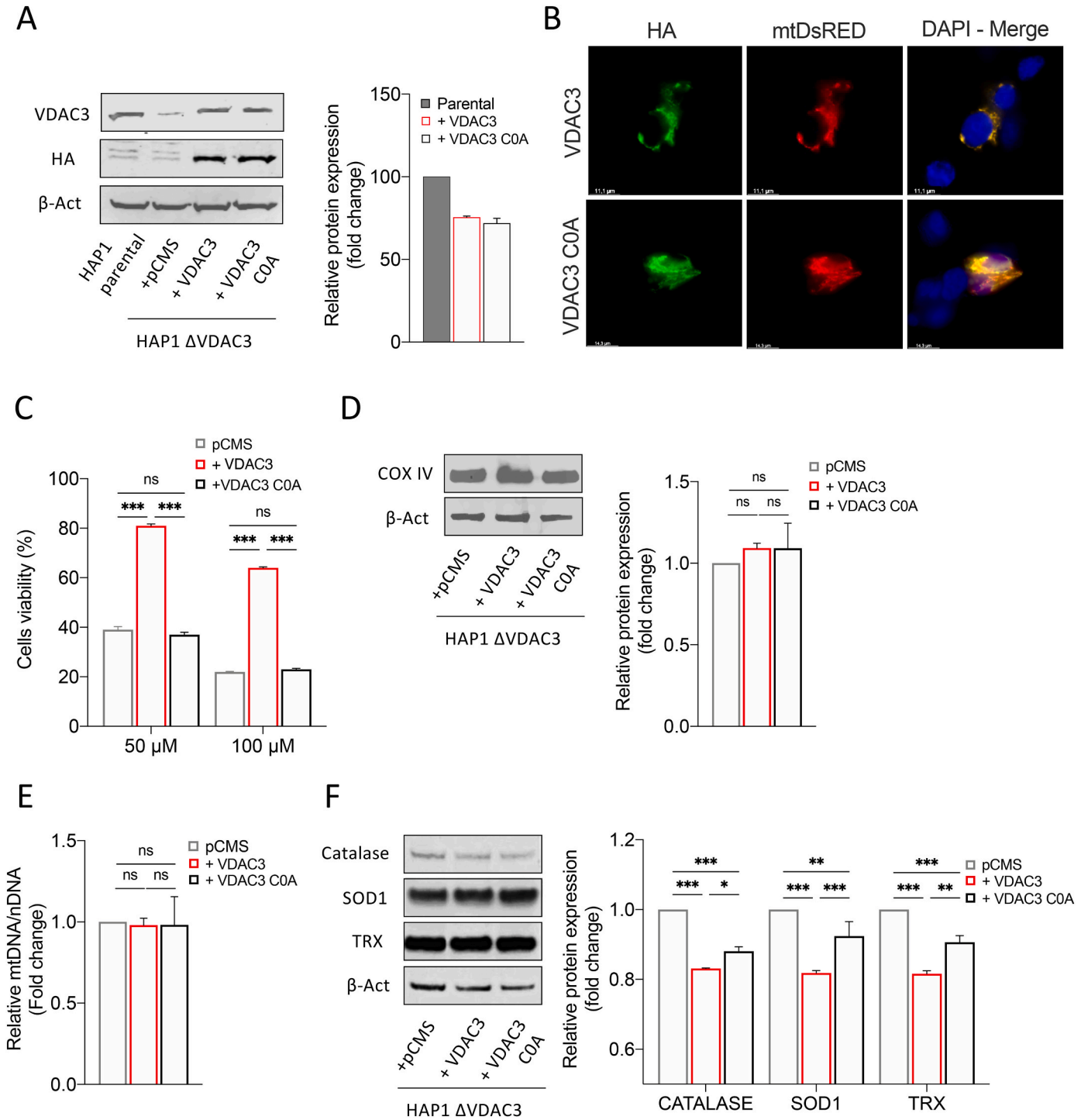

Fig. 4. Evaluation of HAP1-ΔVDAC3 cell profile upon transfection with VDAC3 wild type and VDAC3 *cys-null* mutant. A. Transfection efficiency of HAP1-ΔVDAC3 transfected with VDAC3 wild type (+VDAC3) and VDAC3 cys-null (+VDAC3 C0A) mutant was calculated by relative western blot quantification of VDAC3 proteins in HAP1-ΔVDAC3 compared to the endogenous protein level in HAP1 parental cells. Data were normalized with β-actin, expressed as means ± SEM (n = 3). Anti-HA is shown as control. B. Fluorescence microscopy analysis of subcellular distribution of VDAC3 and VDAC3 C0A in HAP1- ΔVDAC3 by indirect immunofluorescence targeting the HA tag. Mitochondria were visualized by expressing the mitochondrial-targeted mtDsRed protein. Both exogenous proteins are co-localized with mitochondria. C. Cell viability of HAP1-ΔVDAC3 upon transfection with an empty vector (pCMS) or plasmid encoding either for the VDAC3 (+VDAC3) or the VDAC3 C0A (+VDAC3 C0A) and treated with different concentration of rotenone. Data show the mean ± SE (n = 3) and are expressed as a percentage ratio of the treated cells to the untreated ones. D. Quantification of mitochondrial content. Immunoblot illustration and relative quantification of mitochondria-specific protein COX IV level in HAP1-ΔVDAC3 upon transfection. Data are normalized to the β-Actin, expressed as means ± SEM (n = 3) and compared to HAP1-ΔVDAC3 transfected with empty vector. E. Quantification of mtDNA in HAP1-ΔVDAC3 upon transfection. mtDNA amount was measured by Real-Time PCR of the mitochondrial gene COXII and normalized to the nuclear gene APP. Data are expressed as means ± SEM (n = 3) and compared to HAP1-ΔVDAC3 transfected with empty vector. F. Quantification of the main antioxidant enzymes in HAP1-ΔVDAC3 upon transfection. Representative immunoblot and relative protein quantification of Catalase, superoxide dismutase 1 (SOD1) and thioredoxin (TRX). Data are normalized to the β-Actin, expressed as means ± SEM (n = 3) and compared to HAP1-ΔVDAC3 transfected with the empty vector. Data were analyzed with One-Way or Two-Way ANOVA; *$p < 0.05$ **$p < 0.01$ and ***$p < 0.001$.

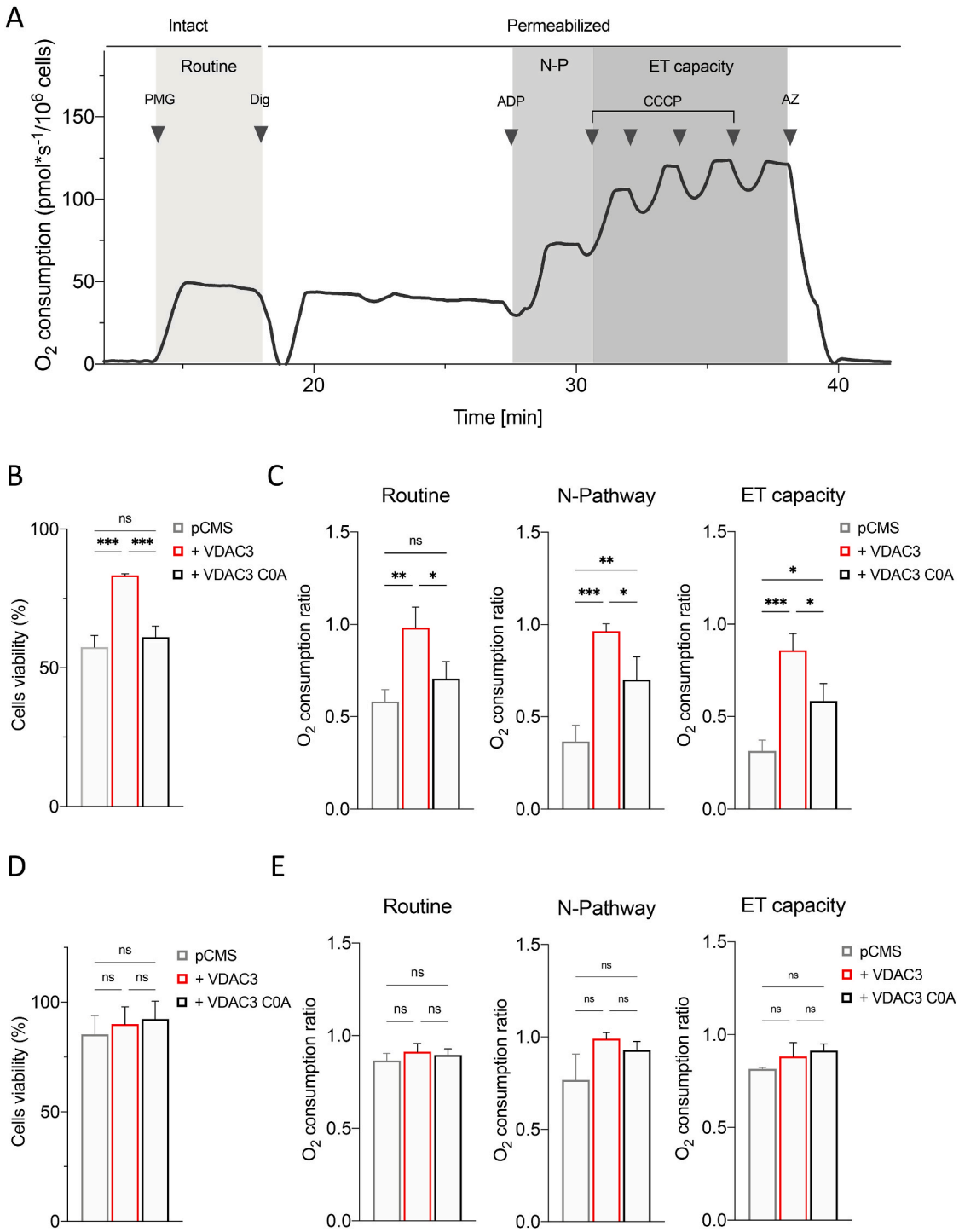

Fig. 5. Oxygen consumption analysis upon rotenone and myxothiazol exposure. A. Representative curve displaying the respirometry profile of untreated HAP1 parental cells and the SUIT protocol applied. The respiratory states Routine, N-pathway and ET capacity were achieved in intact or permeabilized cells with the specific addition of substrates and inhibitors, as following: PMG, pyruvate, malate and glutamate; Dig, digitonin; CCCP, carbonyl cyanide 3-chlorophenylhydrazone; AZ, sodium azide. B. Cell viability of HAP1-ΔVDAC3 upon transfection with an empty vector (pCMS) or plasmid encoding either for the VDAC3 (+VDAC3) or the VDAC3 C0A (+VDAC3 C0A) and treated with 10 nM rotenone. Data show the mean ± SE (n = 3) and are expressed as a percentage ratio of the treated cells to the untreated ones. C. Quantitative analysis of the oxygen consumption in the analyzed states of HAP1-ΔVDAC3 transfected with empty vector (pCMS) or construct carrying VDAC3 (+VDAC3) or VDAC3 C0A mutant (+VDAC3 C0A) attained after the exposure to 10 nM rotenone. Data are indicated as the mean ± SE (n = 3) and expressed as the ratio of the treated cells to the untreated ones. D. Cell viability of HAP1-ΔVDAC3 upon transfection with an empty vector (pCMS) or plasmid encoding either for the VDAC3 (+VDAC3) or the VDAC3 C0A (+VDAC3 C0A) and treated with 10 nM myxothiazol. Data show the mean ± SE (n = 3) and are expressed as a percentage ratio of the treated cells to the untreated ones. E. Quantitative analysis of the oxygen consumption in the analyzed states of HAP1-ΔVDAC3 transfected with empty vector (pCMS) or construct carrying VDAC3 (+VDAC3) or VDAC3 C0A mutant (+VDAC3 C0A) attained after the exposure to 10 nM myxothiazol. Data are indicated as the mean ± SE (n = 3) and expressed as the ratio of the treated cells to the untreated ones. Data were analyzed by one-way ANOVA, with *$p < 0.05$, **$p < 0.01$ and ***$p < 0.001$.

which in turn decreases the utilization of the electrochemical gradient [38]. An alternative interpretation may involve the so-called "incomplete mitochondrial outer membrane permeabilization (MOMP)" which occurs under caspase-inhibited conditions. As widely reported, VDAC1 is essential for mitochondria-mediated apoptosis [18]: for instance, it is required for full processing and activation of caspase-8 [57]. Hence, cells totally devoid of VDAC1 (ΔVDAC1) or carrying a 50% reduction in the expression level of this protein (ΔVDAC3) likely fail to undergo mitochondrial permeabilization. Accordingly, depletion of VDAC1 or VDAC2 by small interfering RNA have been reported to prevent mitochondrial membrane potential dissipation in H460 cells exposed to the cytotoxic isoflavone ME-344 [43]. Moreover, it is worthy of note, that the hyperpolarization of the mitochondrial inner membrane has been demonstrated to anticipate excessive ROS generation [58]. VDAC3 knock out cells effectively disclosed a significant boost in mitochondrial ROS under physiological conditions, as previously observed in H460 cells where VDAC3 was reduced by silencing [43]. This finding perfectly matches with changes in the expression levels of the main intracellular antioxidant enzymes that were all up-regulated within HAP1-ΔVDAC3 cells: this is evidence of an enhanced imbalance between production and accumulation of intracellular ROS. The absence of VDAC1 also increased catalase and thioredoxin expression, although, differently from VDAC3 depletion, down-regulated SOD1 and lowered the basal level of mitochondrial ROS.

Treatments with drugs triggering mitochondrial ROS generation clearly pointed out the extreme vulnerability of cells lacking VDAC3 compared to the control and to the cells devoid of VDAC1. Consistent with these observations, the parental cell line drastically overexpressed VDAC3 in response to prolonged exposure to rotenone, menadione and paraquat, stressing the importance of this specific VDAC isoform in fighting oxidative stress. To this regard, it should be outlined that, under physiological conditions, VDAC3 transcript is the less abundant isoform, despite its promoter retains the greater transcriptional activity compared to those of VDAC1 and VDAC2 [59]. As proposed by Zinghirino et al. [59], this discrepancy could be related to the minor stability of VDAC3 transcripts. Alternatively, cells would maintain the activity of VDAC3 promoter constitutively high in order to promptly increase protein expression upon specific stimuli [59]. However, the mechanism by which VDAC3 is up-regulated following oxidative insults needs to be elucidated: in the light of above, we speculate that this mechanism may include both an increase of mRNA stability and the modulation of gene expression, through the use of a polypyrimidine stretch localized within VDAC3 promoter and identified as a target of oxidative and metabolic stress [60].

Furthermore, HAP1-ΔVDAC3 mitochondria showed the highest increment in superoxide content, upon rotenone and menadione challenge, which proves they failed to counterbalance the overproduction of free-radical species. Rotenone and menadione also induced a sharp collapse of $\Delta\Psi_m$ in these cells suggesting a severe impaired mitochondrial function. Paraquat did not generate the same output, presumably because of VDAC1 down-regulation associated to VDAC3 depletion. VDAC1 is indeed fundamental for paraquat-mediated cytoxicity as, upon toxin-mediated redox cycling, VDAC1-deficient mitochondria experience the lowest amount of superoxide [43]. The role of rotenone, menadione and paraquat-generated mitochondrial ROS in apoptosis has been confirmed [45,61,62]. Our MTT assays proved that, after drug treatments, VDAC3 depletion yields the lowest cell viability compared to the other cell lines. These data, at first suggesting just a greater propension of VDAC3 K.O. cells to apoptosis, are particularly meaningful as removal of isoform 3 is accompanied by the down-regulation of the pro-apoptotic VDAC1 and the up-regulation of the anti-apoptotic VDAC2. Complementation of HAP1-ΔVDAC3, by reintroducing the wild type protein, restored most of the analyzed parameters approximately to levels measured in the HAP1 parental cell line. Interestingly, removal of all cysteine residues abolishes the protective effect of VDAC3 against mitochondrial oxidative damage, leaving only the canonical pore-forming activity [22,23,25,26]. This undoubtedly implies that the involvement of VDAC3 in mitochondrial ROS-sensing is strictly dependent on its cysteine content. HRR measurements of HAP1 cells challenged by ROS producing drugs additionally supported our conclusions. VDAC3 knock out significantly affected mitochondrial respiration of HAP1 cells exposed to rotenone, even at sublethal doses. Interestingly, we found that at nanomolar concentration rotenone promotes only a partial and not significant inhibition of complex I activity, with no effect on cell viability, but a still significative impact for mitochondrial ROS production. 10 nM rotenone had a negligible impact on oxygen flow of HAP1 parental or HAP1-ΔVDAC3 cells transfected with a plasmid encoding VDAC3, while dramatically affecting oxygen consumption of cells transfected with the empty vector. This suggests that VDAC3 is essential for the proper functioning of mitochondria upon oxidative stress. This finding is reinforced by two distinct aspects. First, no comparable effects were observed upon exposure to myxothiazol. Similarly, to rotenone, myxothiazol promoted a significant inhibition of ETS in a dose-dependent manner without increasing mitochondrial ROS production. In this case, the absence of VDAC3 had no effect for oxygen consumption, once again underlining the pivotal role of VDAC3 in counteracting ROS triggered by rotenone. Second, the expression of the cys-null VDAC3 in HAP1-ΔVDAC3 cells did not restore the physiological oxygen flow in presence of endogenous substrates, while partially improved oxygen consumption of permeabilized VDAC3 knock out cells. This indicates that the absence of cysteine residues makes VDAC3 unable to efficiently counteract the rotenone effect. The partial improvement in oxygen flows here observed could depends on the cys-null mutant ability to form canonical VDAC-like channels [23,26]. It has been recently shown that VDAC overexpression counteracts mitochondrial respiratory impairment by increasing the availability of adenylates and substrates. As a result, the respiration was overall improved [63]. Anyhow, cys-null VDAC3 is not able to fully recover oxygen flow as VDAC3, and this strengthens once again the pivotal role exerted by cysteine residues.

In conclusion, as hypothesized before [29–31], we demonstrate that VDAC3 protects mitochondria from oxidative stress-induced impairment, although the underlying molecular mechanism remains elusive. In particular, experimental results obtained with the VDAC3 mutant completely devoid of cysteine residues suggest that these amino acids are crucial for the protein ability to perceives changes in the amount of mitochondrial reactive oxygen species. Accumulation of oxidative modifications within VDAC3 cysteines may be used indeed as a *redox--state marker* of mitochondria by inducing conformational changes which, in turn, could signal the ROS load of the single mitochondrion to other proteins or organelles. Accordingly, VDAC3 could contribute to mitochondrial quality control in two ways: i) over-oxidated VDAC3 may undergo ubiquitination [64] and promote the clearance of defective mitochondria or, ii), ROS-induced conformational changes could drive protein incorporation into membranous structures secreted by mitochondria under oxidative stress called mitochondria-derived vesicles (MDVs), that participate in maintaining a healthy and functional mitochondrial network. Another possible explanation is that, in response to increased levels of mitochondrial ROS, VDAC3 is "sacrified" through the retro-translocation pathway (N-end rule pathway) which translocates a protein containing an oxidated N-terminal cysteine (i.e. VDAC3 contains a cys in position 2 which becomes the actual N-terminal residue following removal of the starting methionine) to the cytosolic proteasome for its degradation [12]. The lack of evidence of VDAC3 cys2 oxidation, suggests, that indeed, each protein containing this altered amino acid residue could be immediately destroyed by the N-end rule pathway. To this regard, Messina et al. [32], identified the valosin-containing protein (VCP) also known as transitional endoplasmic reticulum ATPase (TER ATPase) or p97 in mammals, as a VDAC3 interactor. VCP is part of the ubiquitin-proteasome system [65] and is also required for the proper functioning of the lysosomal system and autophagy [66], hence it is involved in the "extraction" of proteins

from the outer mitochondrial membrane (OMM) and other membranes to be subsequently ubiquitinated and degraded.

4. Methods

4.1. Cell culture and treatment

Near-haploid human HAP1 cell (C631), and derived cell lines HAP1 VDAC1 knock out (HZGHC005706c002) and HAP1 VDAC3 knock out (HZGHC005689c006) cells were obtained from Horizon Discovery. Knockout clones were edited by CTRISPR/Cas system. VDAC1 knock out clone contains a 2 pb deletion in exon 6 while, VDAC3 knock out clone contains a 17 bp deletion in exon 7. HAP1 cell lines were maintained at 37 °C in the presence of 5% CO2 in Iscove's modified Dulbecco's media (IMDM) supplemented with 10% (v/v) fetal bovine serum (FBS), 100 U/ml penicillin and 100 μg/ml streptomycin. Each cell line was treated with different compound: Menadione (15 or 25 μM dissolved in 0,01% DMSO) for 3 h; Rotenone (50 or 100 μM dissolved in 0,01% DMSO) for 24 h and Paraquat (50, 100 or 500 μM dissolved in H_2O) for 24 h. Subsequently, the cells were used for cell viability assay describe below.

4.2. Cell viability assay

Cell viability was evaluated by 3-(4,5-dimethylthiazolyl-2)-2,5-diphenyltetrazoliumbromide (MTT) assay. HAP1 cell lines were plated in 96-well plates at 10,000 cell/well and after 24 h received the indicated treatment. Subsequently, MTT was added to the culture medium to reach final concentration of 5 mg/ml. After incubation at 37 °C for 3 h, the medium was removed and the formazan crystals produced were dissolved by adding 100 μl of dimethyl sulfoxide. The absorbance at 590 nm was determined using the microplates reader Varioskan (Thermo Scientific). Data were statistically analyzed by two-way ANOVA followed by Dunnett's multiple comparisons test.

4.3. Quantitative Real-time PCR

Quantitative Real-time PCR was used to analyze the level of expression of the following genes: VDAC1, VDAC2, VDAC3, NRF-1, TFAM, PCG-1α. Total RNA was extracted using TRIzol® Reagent (ThermoFisher Scientific) according to manufacturer's instructions. RNA concentration and purity were measured by a spectrophotometer and 1 μg was used to synthesize cDNA by QuantiTect Reverse Transcription kit (Qiagen). For each experiment, three independent Real-Time PCR runs were performed in triplicate using the QuantiTec SYBR Green PCR Kit (QIAGEN). Analysis was performed in the Mastercycler ep realplex (Eppendorf) in 96-well plates. Thermocycling program consisted in a first activation at 95 °C for 15 min, followed by 40 cycles at 95 °C for 15 s, annealing at 57 °C for 15 s, extension at 68 °C for 15 s and a final step at 72 °C for 10 min. Analysis of relative expression level was performed using the housekeeping β-actin gene as internal calibrator by the ΔΔCt method [67]. Data were statistically analyzed by one-way ANOVA followed by Dunnett's multiple comparisons test.

4.4. Mitochondrial DNA analysis

To determinate the relative amount of mitochondrial DNA in the HAP1 cell lines, total DNA was extracted as described in Ref. [68]. Briefly, total DNA (20 ng) was used as a template in real-time PCR with primers for the COXII gene in mitochondrial DNA and nuclear gene for APP. Analysis of mtDNA/nDNA ratio was calculated by following the classical ΔΔCt method. Data were statistically analyzed by one-way ANOVA.

4.5. Measurement of the mitochondrial membrane potential, mitochondrial mass and mitochondrial superoxide

$\Delta\Psi_m$ was measured using alternatively two different probes suitable for determining mitochondrial membrane potential changes: tetramethyl-rhodamine methyl ester (TMRM), and Mito Tracker red. Both probes accumulate into active mitochondria due their positive charge whereby the reduction of $\Delta\Psi_m$ leads to the release of them. Conventional fluorescent stains for mitochondria, such as TMRM, are readily sequestered by functioning mitochondria and they are subsequently washed out of the cells once the mitochondrion's membrane potential is lost. This characteristic makes TMRM very useful in experiments where sudden changes must be detected. However, when using dual staining of mitochondria, TMRM should be used paying attention to its spectral features. Here we used the Mito Tracker Green (ThermoFisher) probe that allow measurements of mitochondrial mass being a probe that accumulates into mitochondria independently of the mitochondrial membrane potential status. Thus, when using flow cytometry, values measured for mitochondrial membrane potential could be normalized to the mitochondrial content per cell. In this case, to avoid false interpretation of results due to the overlap between Mito tracker Green emission spectrum and TMRM excitation spectrum, we used Mito tracker red, because of its spectral properties which allow a better signal detection when using simultaneously to others green probes.

After treatments, adherent cells were washed with PBS and then incubated for 30 min at 37 °C with Krebs Ringer Buffered Saline (130 mM NaCl, 3.6 mM KCl, 10 mM HEPES, 2 mM $NaHCO_3$, 0.5 mM NaH_2PO_4, 0.5 mM $MgCl_2$, 1.5 mM $CaCl_2$, 4.5 g/l glucose, pH 7.42) supplemented with mitochondrial probes (either 200 nM TMRM or 300 nM Mito tracker Green and 300 nm Mito tracker Red). In all cases 20 μM verapamil were added as a multi drug-resistant pump inhibitor (Sigma). Cells were then detached by a short treatment with trypsin–EDTA, resuspended in the above described buffer, supplemented with 1% FCS to neutralize the trypsin and immediately analyzed on a CyFlow® ML flow cytometer (Partec) in FL3 and FL1 log mode. Only viable cells detected by reading the scattering indicated as FSC and SSC, were considered for our analysis.The threshold physiological value of $\Delta\Psi_m$ was estimated by using cells exposed to 10 μM of the uncoupling agent FCCP as a negative control. Compensation algorithms were applied between FL1 and FL3 channels, when signals from Mito tracker Green and Mito tracker Red were read in the same cells, to normalize $\Delta\Psi_m$/mitochondrion/cell.

Mitochondrial superoxide, was measured by using MitoSOX Red (ThermoFisher) whose specificity for superoxide has been shown by the manufacturer. Briefly, cells were stained with 5 μM MitoSOX Red in Krebs Ringer Buffered Saline for 10 min at 37 °C, and FL2 median fluorescence intensity was measured by flow cytometry.

4.6. Growth curve

The day 0, 80000 cells from each HPA1 cell lines (parental, DVDAC1 and DVADC3) were seeded in 12 well plates. Then cells were collected and counted each 24h for 5 days by using flow cytometry. The CyFlow® ML analyses concentrations of any particle or cell subpopulations of interest using True Volumetric Absolute Counting. This unique method is solely based on the fundamental definition of absolute counting respectively the particle concentration (c) which is equal to the counted number (N) of particles (e.g. cells) in a given volume (V), $c = N/V$. In the CyFlow® ML, the volume is measured directly by mechanical means, rather than by calibration with expensive beads eliminating any errors related to varying bead concentrations or bead aggregation. The CyFlow® ML allows the analysis of a fixed volume as defined by the distance between two platinum electrodes reaching into the sample tube with a given diameter.

4.7. Flow cytometry

20,000 cells per sample were analyzed using a CyFlow® ML flow cytometer (Partec) system equipped with three laser sources and 10 optical parameters with dedicated filter settings and a high numerical aperture microscope objective (50 × NA 0.82) for the detection of different scatter and fluorescence signals. The cells were excited by an air-cooled argon 488 nm laser and then the signal from Mitotracker Green was read on FL1, Mitosox on FL2, detectors while the signal from TMRM, Mitotracker Red DsRed on FL3 detector. Data obtained were acquired, gated, compensated, and analyzed using the FlowMax software (Partec) and FCS Express 4 software (DeNovo). Data reported were obtained for three sets of independent experiments, each performed in triplicate and based on 20,000 events for each group. Cytometric profiles reported in each Figure are representative of one of the three sets of measurements. Data were statistical analyzed by chi-square test. A $p < 0,001$ was taken as significant.

4.8. Western blots

1×10^6 cells for each line were collected and lysed in extraction buffer (50 mM Tris pH 7.4, 150 mM NaCl, EDTA 1 mM, 1% TRITON X-100 and protease inhibitors). After lysis, the supernatant was collected and the protein content was measured in triplicate using the Bradford reagent with bovine serum albumin (BSA) as a standard. 50 μg of total protein of each sample were separated using SDS/PAGE electrophoresis, transferred to a PDVF membrane (Amersham Hybond P 0.45; GE Healthcare Life Sciences) and blocked in 2,5% BSA at room temperature for 1h. The membranes were incubated overnight at 4 °C with primary antibodies against VDAC1 (1:1000, ab34726, Abcam), VDAC1 (1:200, ab154856, Abcam), VDAC2 (1:300, ab37985, Abcam), VDAC3 (1:100, ab130561, Abcam), COX IV (1:3000 #3E11, Cell Signaling Technology), HA-Tag (1:1000, #3724, Cell Signaling Technology), Oxidative Stress Defense (Catalase, SOD1, TRX, smooth muscle Actin) western blot cocktail (1:1000, ab179843, Abcam), SDHA (1:000, ab14715, Abcam), β-Actin (1:1000, #3700, Cell Signaling Technology), β-Tubulin (1:2000, #2146, Cell Signaling Technology) and after the washing step with secondary antibodies IRDye® 800CW Donkey anti-Mouse IgG (1:20000, 926–32212, Li-Cor Biosciences), IRDye® 680RD Donkey anti-Rabbit IgG (1:20000, 926–68073, Li-Cor Biosciences) and IRDye® 800CW Donkey anti-Goat IgG (1:20000, 926–32214, Li-Cor Biosciences). The membranes were scanned using the Odyssey CLx imaging system (Li-Cor Biosciences). Data were analyzed with ImageStudioLite software (Li-Cor Biosciences) and β-Tubulin or β-Actin was used as an internal control for normalizing protein loading. Data were statistically analyzed by one-way ANOVA followed by Dunnett's multiple comparisons test.

4.9. Cell transfection

HAP1 ΔVDAC3 cells were transfected with the pCMS-MtDsRed [69] carrying the encoding sequence of human VDAC3 or VDAC3 C0A in frame with the HA-tag at the C-terminus. The empty pCMS plasmid was used as control. Cells were seeded in a 6-well or 96-well plates and transfected using 5 μg DNA per well by Lipofectamine 3000 (Life Technologies) according to manufacturer's instructions. Further analyzes were performed after 48 h.

4.10. Indirect immunofluorescence of adherent cells

In order to detect the expression of VDAC3, following transfection with pCMS-MtDsRed-VDAC3-HA, we used indirect immunofluorescence. 48h post-transfection, cells growth on coverslips, were fixed in 4% formaldehyde, washed three times in PBS 1x, and incubated 10 min in 50 mM NH_4Cl. Cells were then permeabilized by using 0.3% Triton X-100. Unspecific binding was blocked by 30 min in 0.2% gelatine in PBS. To detect the expression and localization of VDAC3-HA in mtDsRed overexpressing cells, coverslips were incubated overnight with anti-HA (rabbit 1:100, Santa Cruz Biotechnology, Inc.). After PBS washing, cells were exposed for 1h at RT to the secondary anti-rabbit antibody AlexaFluor 488. After PBS washing, cells were exposed for 1 h at RT to the secondary antibody (anti-rabbit 1:2000, ThermoFischer). Coverslips were mounted by using DAPI-Fluoromount-G to stain nuclear DNA. Co-localization with mitochondria was obtained by merging the HA signal with the signal from the fluorescent reporter mtDsRed. A Leica DMI 6000B epifluorescence inverted microscope with Adaptive Focus Control was used. This system is outfitted with a controllable X-cite mercury lamp and an extensive collection of filter cubes (360, 488, 560, 604 nm excitation) for fluorescent microscopy, and a halogen lamp for bright field and DIC. It is equipped with 4 bright lenses (10, 20, 40, 63x), a high-resolution Hamamatsu Orca R2 CCD camera (1344 × 1024 pixels), and motorized stage (XY only). Images were obtained by using the Leica LAS Extended Annotation software.

4.11. High-Resolution Respirometry

Effect of rotenone and myxothiazol for the respiratory capacity of parental or ΔVDAC3 HAP1 cells was investigated by High-Resolution Respirometry using the two-chamber system O2k-FluoRespirometer (Oroboros Instruments). Parental HAP1 were exposed for 24 h to increasing concentration of rotenone or myxothiazol ranging from 10 nM to 10 μM. 24 h transfected ΔVDAC3 HAP1 cells were incubated with 10 nM rotenone, 10 nM myxothiazol or DMSO for additional 24 h and the respiratory states were then determined by a specific substrate-uncoupler-inhibitor titration (SUIT) protocol modified from Ref. [58]. Briefly, oxygen consumption in intact cells was first analyzed. Next, plasma membranes were permeabilized with 4 μM digitonin, without disturbing mitochondrial membranes, and the oxygen flow related to oxidative phosphorylation driven by the complex I activity (N-pathway) was attained by the addition of pyruvate (5 mM), glutamate (10 mM), malate (2 mM) and ADP (2.5 mM). The maximal capacity of electron transport (ET) was finally determined by titration with the uncoupler carbonyl cyanide 3-chlorophenylhydrazone (CCCP, 0.5 μM) up to the complete dissipation of the proton gradient. The activity of the respiratory chain enzymes was inhibited by the addition of 100 mM sodium azide. All substrates were purchased by Sigma Aldrich.

At least three independent experiments for each condition tested were performed in mitochondrial respiration buffer Mir05 (Oroboros Instruments) at 37 °C under constant stirring of 750 rpm. Instrumental and chemical background fluxes were calibrated as a function of the oxygen concentration using DatLab software (Oroboros Instruments). Oxygen consumption in intact cells or correspondent to N-pathway and maximal ET capacity in cells exposed to rotenone or myxothiazol was expressed as pmol/s per million cells and normalized to their respective untreated controls.

4.12. Statistical analysis

Data are presented as mean ± standard error of the mean (SEM). Dependent variables were analyzed by one-way or two-way ANOVA followed by Dunnett's multiple comparisons test using GraphPad Prism version 9.0.0 (GraphPad Software, San Diego, California USA). A value of $P < 0.05$ was considered significant. In particular, * indicates a $P < 0.05$, ** indicates a $P < 0.01$, *** indicates a $P < 0.001$.

Author contributions

S.R. designed and supervised the experiments and analyzed the results. S.C.N. performed cell cultures, western blot and prepared figures. M.F.T. performed the flow cytometry experiments. A. Magrì conducted the high resolution respirometry measurements. S.R. and V.D.P wrote the original draft of the manuscript. M.F.T., A. Magrì., S.C.N. and A. Messina reviewed and edited the text. The authors acknowledge Rigel

Villagonzalo Rountree for language editing.

Fundings

The authors acknowledge funding by the Italian Ministry of University and Research to project Proof of Concept 2018, grant number PEPSLA POC 01_00054 (to A.M.), the University of Catania - linea PIACERI, grant number ARVEST (to A.M) and the AIM Linea 1-Salute (AIM1833071).

Declaration of competing interest

The authors declare that they have no affiliations with or involvement in any organization or entity with any financial interest (such as honoraria; educational grants; participation in speakers' bureaus; membership, employment, consultancies, stock ownership, or other equity interest; and expert testimony or patent-licensing arrangements), or non-financial interest (such as personal or professional relationships, affiliations, knowledge or beliefs) in the subject matter or materials discussed in this manuscript.

Appendix A. Supplementary data

Supplementary data to this article can be found online at https://doi.org/10.1016/j.redox.2022.102264.

References

[1] J.F. Turrens, Mitochondrial formation of reactive oxygen species, J. Physiol. 552 (2003) 335–344, https://doi.org/10.1113/jphysiol.2003.049478.
[2] R.S. Balaban, S. Nemoto, T. Finkel, Mitochondria, oxidants, and aging, Cell 120 (2005) 483–495, https://doi.org/10.1016/j.cell.2005.02.001.
[3] V. Adam-Vizi, C. Chinopoulos, Bioenergetics and the formation of mitochondrial reactive oxygen species, Trends Pharmacol. Sci. 27 (2006) 639–645, https://doi.org/10.1016/j.tips.2006.10.005.
[4] M.P. Murphy, Mitochondrial thiols in antioxidant protection and redox signaling: distinct roles for glutathionylation and other thiol modifications, Antioxidants Redox Signal. 16 (2012) 476–495, https://doi.org/10.1089/ars.2011.4289.
[5] E.-M. Hanschmann, J.R. Godoy, C. Berndt, C. Hudemann, C.H. Lillig, Thioredoxins, glutaredoxins, and peroxiredoxins–molecular mechanisms and health significance: from cofactors to antioxidants to redox signaling, Antioxidants Redox Signal. 19 (2013) 1539–1605, https://doi.org/10.1089/ars.2012.4599.
[6] J.N. Peoples, A. Saraf, N. Ghazal, T.T. Pham, J.Q. Kwong, Mitochondrial dysfunction and oxidative stress in heart disease, Exp. Mol. Med. 51 (2019) 1–13, https://doi.org/10.1038/s12276-019-0355-7.
[7] W.-X. Ding, X.-M. Yin, Mitophagy: mechanisms, pathophysiological roles, and analysis, Biol. Chem. 393 (2012) 547–564, https://doi.org/10.1515/hsz-2012-0119.
[8] T. Shpilka, C.M. Haynes, The mitochondrial UPR: mechanisms, physiological functions and implications in ageing, Nat. Rev. Mol. Cell Biol. 19 (2018) 109–120, https://doi.org/10.1038/nrm.2017.110.
[9] P. Storz, H. Döppler, A. Toker, Protein kinase D mediates mitochondrion-to-nucleus signaling and detoxification from mitochondrial reactive oxygen species, Mol. Cell Biol. 25 (2005) 8520–8530, https://doi.org/10.1128/MCB.25.19.8520-8530.2005.
[10] P. Storz, Mitochondrial ROS–radical detoxification, mediated by protein kinase D, Trends Cell Biol. 17 (2007) 13–18, https://doi.org/10.1016/j.tcb.2006.11.003.
[11] S. Reina, V. Checchetto, R. Saletti, A. Gupta, D. Chaturvedi, C. Guardiani, F. Guarino, M.A. Scorciapino, A. Magrì, S. Foti, M. Ceccarelli, A.A. Messina, R. Mahalakshmi, I. Szabo, V. De Pinto, VDAC3 as a sensor of oxidative state of the intermembrane space of mitochondria: the putative role of cysteine residue modifications, Oncotarget 7 (2016) 2249–2268, https://doi.org/10.18632/oncotarget.6850.
[12] S. Reina, F. Guarino, A. Magrì, V. De Pinto, VDAC3 as a potential marker of mitochondrial status is involved in cancer and pathology, Front. Oncol. 6 (2016) 264, https://doi.org/10.3389/fonc.2016.00264.
[13] M.C. Brahimi-Horn, S. Giuliano, E. Saland, S. Lacas-Gervais, T. Sheiko, J. Pelletier, I. Bourget, F. Bost, C. Féral, E. Boulter, M. Tauc, M. Ivan, B. Garmy-Susini, A. Popa, B. Mari, J.-E. Sarry, W.J. Craigen, J. Pouysségur, N.M. Mazure, Knockout of Vdac1 activates hypoxia-inducible factor through reactive oxygen species generation and induces tumor growth by promoting metabolic reprogramming and inflammation, Cancer Metabol. 3 (2015) 8, https://doi.org/10.1186/s40170-015-0133-5.
[14] D. Han, F. Antunes, R. Canali, D. Rettori, E. Cadenas, Voltage-dependent anion channels control the release of the superoxide anion from mitochondria to cytosol, J. Biol. Chem. 278 (2003) 5557–5563, https://doi.org/10.1074/jbc.M210269200.
[15] N. Roos, R. Benz, D. Brdiczka, Identification and characterization of the pore-forming protein in the outer membrane of rat liver mitochondria, Biochim. Biophys. Acta 686 (1982) 204–214, https://doi.org/10.1016/0005-2736(82)90114-6.
[16] M. Colombini, E. Blachly-Dyson, M. Forte, VDAC, a channel in the outer mitochondrial membrane, Ion Channel. 4 (1996) 169–202, https://doi.org/10.1007/978-1-4899-1775-1_5.
[17] G.C. Shore, Apoptosis: it's BAK to VDAC, EMBO Rep. 10 (2009) 1311–1313, https://doi.org/10.1038/embor.2009.249.
[18] V. Shoshan-Barmatz, E.N. Maldonado, Y. Krelin, VDAC1 at the crossroads of cell metabolism, apoptosis and cell stress, Cell Stress 1 (2017) 11–36, https://doi.org/10.15698/cst2017.10.104.
[19] A. Messina, S. Reina, F. Guarino, V. De Pinto, VDAC isoforms in mammals, Biochim. Biophys. Acta 1818 (2012) 1466–1476, https://doi.org/10.1016/j.bbamem.2011.10.005.
[20] R. Benz, Permeation of hydrophilic solutes through mitochondrial outer membranes: review on mitochondrial porins, Biochim. Biophys. Acta 1197 (1994) 167–196, https://doi.org/10.1016/0304-4157(94)90004-3.
[21] X. Xu, W. Decker, M.J. Sampson, W.J. Craigen, M. Colombini, Mouse VDAC isoforms expressed in yeast: channel properties and their roles in mitochondrial outer membrane permeability, J. Membr. Biol. 170 (1999) 89–102, https://doi.org/10.1007/s002329900540.
[22] V. Checchetto, S. Reina, A. Magrì, I. Szabo, V. De Pinto, Recombinant human voltage dependent anion selective channel isoform 3 (hVDAC3) forms pores with a very small conductance, Cell. Physiol. Biochem. 34 (2014) 842–853, https://doi.org/10.1159/000363047.
[23] M. Queralt-Martín, L. Bergdoll, O. Teijido, N. Munshi, D. Jacobs, A.J. Kuszak, O. Protchenko, S. Reina, A. Magrì, V. De Pinto, S.M. Bezrukov, J. Abramson, T. K. Rostovtseva, A lower affinity to cytosolic proteins reveals VDAC3 isoform-specific role in mitochondrial biology, J. Gen. Physiol. 152 (2020), e201912501, https://doi.org/10.1085/jgp.201912501.
[24] S. Conti Nibali, M.C. Di Rosa, O. Rauh, G. Thiel, S. Reina, V. De Pinto, Cell-free electrophysiology of human VDACs incorporated into nanodiscs: an improved method, Biophys Rep 1 (2021), https://doi.org/10.1016/j.bpr.2021.100002. None.
[25] S. Reina, V. Palermo, A. Guarnera, F. Guarino, A. Messina, C. Mazzoni, V. De Pinto, Swapping of the N-terminus of VDAC1 with VDAC3 restores full activity of the channel and confers anti-aging features to the cell, FEBS Lett. 584 (2010) 2837–2844, https://doi.org/10.1016/j.febslet.2010.04.066.
[26] S. Reina, V. Checchetto, R. Saletti, A. Gupta, D. Chaturvedi, C. Guardiani, F. Guarino, M.A. Scorciapino, A. Magrì, S. Foti, M. Ceccarelli, A.A. Messina, R. Mahalakshmi, I. Szabo, V. De Pinto, VDAC3 as a sensor of oxidative state of the intermembrane space of mitochondria: the putative role of cysteine residue modifications, Oncotarget 7 (2016) 2249–2268, https://doi.org/10.18632/oncotarget.6850.
[27] M. Okazaki, K. Kurabayashi, M. Asanuma, Y. Saito, K. Dodo, M. Sodeoka, VDAC3 gating is activated by suppression of disulfide-bond formation between the N-terminal region and the bottom of the pore, Biochim. Biophys. Acta 1848 (2015) 3188–3196, https://doi.org/10.1016/j.bbamem.2015.09.017.
[28] V. De Pinto, S. Reina, A. Gupta, A. Messina, R. Mahalakshmi, Role of cysteines in mammalian VDAC isoforms' function, Biochim. Biophys. Acta 1857 (2016) 1219–1227, https://doi.org/10.1016/j.bbabio.2016.02.020.
[29] S. Reina, M.G.G. Pittalà, F. Guarino, A. Messina, V. De Pinto, S. Foti, R. Saletti, Cysteine oxidations in mitochondrial membrane proteins: the case of VDAC isoforms in mammals, Front. Cell Dev. Biol. 8 (2020) 397, https://doi.org/10.3389/fcell.2020.00397.
[30] R. Saletti, S. Reina, M.G.G. Pittalà, R. Belfiore, V. Cunsolo, A. Messina, V. De Pinto, S. Foti, High resolution mass spectrometry characterization of the oxidation pattern of methionine and cysteine residues in rat liver mitochondria voltage-dependent anion selective channel 3 (VDAC3), Biochim. Biophys. Acta Biomembr. 1859 (2017) 301–311, https://doi.org/10.1016/j.bbamem.2016.12.003.
[31] M.G.G. Pittalà, R. Saletti, S. Reina, V. Cunsolo, V. De Pinto, S. Foti, A high resolution mass spectrometry study reveals the potential of disulfide formation in human mitochondrial voltage-dependent anion selective channel isoforms (hVDACs), Int. J. Mol. Sci. 21 (2020) E1468, https://doi.org/10.3390/ijms21041468.
[32] A. Messina, S. Reina, F. Guarino, A. Magrì, F. Tomasello, R.E. Clark, R.R. Ramsay, V. De Pinto, Live cell interactome of the human voltage dependent anion channel 3 (VDAC3) revealed in HeLa cells by affinity purification tag technique, Mol. Biosyst. 10 (2014) 2134–2145, https://doi.org/10.1039/c4mb00237g.
[33] L. Bleier, I. Wittig, H. Heide, M. Steger, U. Brandt, S. Dröse, Generator-specific targets of mitochondrial reactive oxygen species, Free Radic. Biol. Med. 78 (2015) 1–10, https://doi.org/10.1016/j.freeradbiomed.2014.10.511.
[34] L. Zou, V. Linck, Y.-J. Zhai, L. Galarza-Paez, L. Li, Q. Yue, O. Al-Khalili, H.-F. Bao, H.-P. Ma, T.L. Thai, J. Jiao, D.C. Eaton, Knockout of mitochondrial voltage-dependent anion channel type 3 increases reactive oxygen species (ROS) levels and alters renal sodium transport, J. Biol. Chem. 293 (2018) 1666–1675, https://doi.org/10.1074/jbc.M117.798645.
[35] P. Jóźwiak, P. Ciesielski, E. Forma, K. Kozal, K. Wójcik-Krowiranda, Ł. Cwonda, A. Bieńkiewicz, M. Bryś, A. Krześlak, Expression of voltage-dependent anion channels in endometrial cancer and its potential prognostic significance, Tumour Biol. 42 (2020), https://doi.org/10.1177/1010428320951057, 1010428320951057.
[36] C. Lee, J.S. Nam, C.G. Lee, M. Park, C.-M. Yoo, H.-W. Rhee, J.K. Seo, T.-H. Kwon, Analysing the mechanism of mitochondrial oxidation-induced cell death using a multifunctional iridium(III) photosensitiser, Nat. Commun. 12 (2021) 26, https://doi.org/10.1038/s41467-020-20210-3.

[37] A. Magrì, M.C. Di Rosa, I. Orlandi, F. Guarino, S. Reina, M. Guarnaccia, G. Morello, A. Spampinato, S. Cavallaro, A. Messina, M. Vai, V. De Pinto, Deletion of Voltage-Dependent Anion Channel 1 knocks mitochondria down triggering metabolic rewiring in yeast, Cell. Mol. Life Sci. 77 (2020) 3195–3213, https://doi.org/10.1007/s00018-019-03342-8.
[38] A. Perl, P. Gergely, G. Nagy, A. Koncz, K. Banki, Mitochondrial hyperpolarization: a checkpoint of T-cell life, death and autoimmunity, Trends Immunol. 25 (2004) 360–367, https://doi.org/10.1016/j.it.2004.05.001.
[39] M.S. Baghel, M.K. Thakur, Vdac1 downregulation causes mitochondrial disintegration leading to hippocampal neurodegeneration in scopolamine-induced amnesic mice, Mol. Neurobiol. 56 (2019) 1707–1718, https://doi.org/10.1007/s12035-018-1164-z.
[40] N. Tajeddine, L. Galluzzi, O. Kepp, E. Hangen, E. Morselli, L. Senovilla, N. Araujo, G. Pinna, N. Larochette, N. Zamzami, N. Modjtahedi, A. Harel-Bellan, G. Kroemer, Hierarchical involvement of Bak, VDAC1 and Bax in cisplatin-induced cell death, Oncogene 27 (2008) 4221–4232, https://doi.org/10.1038/onc.2008.63.
[41] F. Tomasello, A. Messina, L. Lartigue, L. Schembri, C. Medina, S. Reina, D. Thoraval, M. Crouzet, F. Ichas, V. De Pinto, F. De Giorgi, Outer membrane VDAC1 controls permeability transition of the inner mitochondrial membrane in cellulo during stress-induced apoptosis, Cell Res. 19 (2009) 1363–1376, https://doi.org/10.1038/cr.2009.98.
[42] A. Tikunov, C.B. Johnson, P. Pediaditakis, N. Markevich, J.M. Macdonald, J. J. Lemasters, E. Holmuhamedov, Closure of VDAC causes oxidative stress and accelerates the Ca(2+)-induced mitochondrial permeability transition in rat liver mitochondria, Arch. Biochem. Biophys. 495 (2010) 174–181, https://doi.org/10.1016/j.abb.2010.01.008.
[43] L. Zhang, D.M. Townsend, M. Morris, E.N. Maldonado, Y.-L. Jiang, A.-M. Broome, J.R. Bethard, L.E. Ball, K.D. Tew, Voltage-dependent anion channels influence cytotoxicity of ME-344, a therapeutic isoflavone, J. Pharmacol. Exp. Therapeut. 374 (2020) 308–318, https://doi.org/10.1124/jpet.120.000009.
[44] H. Shimada, K.-I. Hirai, E. Simamura, T. Hatta, H. Iwakiri, K. Mizuki, T. Hatta, T. Sawasaki, S. Matsunaga, Y. Endo, S. Shimizu, Paraquat toxicity induced by voltage-dependent anion channel 1 acts as an NADH-dependent oxidoreductase, J. Biol. Chem. 284 (2009) 28642–28649, https://doi.org/10.1074/jbc.M109.033431.
[45] N. Li, K. Ragheb, G. Lawler, J. Sturgis, B. Rajwa, J.A. Melendez, J.P. Robinson, Mitochondrial complex I inhibitor rotenone induces apoptosis through enhancing mitochondrial reactive oxygen species production, J. Biol. Chem. 278 (2003) 8516–8525, https://doi.org/10.1074/jbc.M210432200.
[46] A.A. Starkov, G. Fiskum, Regulation of brain mitochondrial H2O2 production by membrane potential and NAD(P)H redox state, J. Neurochem. 86 (2003) 1101–1107, https://doi.org/10.1046/j.1471-4159.2003.01908.x.
[47] T. Tron, M. Crimi, A.M. Colson, M. Degli Esposti, Structure/function relationships in mitochondrial cytochrome b revealed by the kinetic and circular dichroic properties of two yeast inhibitor-resistant mutants, Eur. J. Biochem. 199 (1991) 753–760, https://doi.org/10.1111/j.1432-1033.1991.tb16180.x.
[48] A.M. Gusdon, G.A. Fernandez-Bueno, S. Wohlgemuth, J. Fernandez, J. Chen, C. E. Mathews, Respiration and substrate transport rates as well as reactive oxygen species production distinguish mitochondria from brain and liver, BMC Biochem. 16 (2015) 22, https://doi.org/10.1186/s12858-015-0051-8.
[49] T.V. Votyakova, I.J. Reynolds, ΔΨm-Dependent and -independent production of reactive oxygen species by rat brain mitochondria, J. Neurochem. 79 (2001) 266–277, https://doi.org/10.1046/j.1471-4159.2001.00548.x.
[50] J.F. Turrens, A. Alexandre, A.L. Lehninger, Ubisemiquinone is the electron donor for superoxide formation by complex III of heart mitochondria, Arch. Biochem. Biophys. 237 (1985) 408–414, https://doi.org/10.1016/0003-9861(85)90293-0.
[51] J. Vergalli, I.V. Bodrenko, M. Masi, L. Moynié, S. Acosta-Gutiérrez, J.H. Naismith, A. Davin-Regli, M. Ceccarelli, B. van den Berg, M. Winterhalter, J.-M. Pagès, Porins and small-molecule translocation across the outer membrane of Gram-negative bacteria, Nat. Rev. Microbiol. 18 (2020) 164–176, https://doi.org/10.1038/s41579-019-0294-2.
[52] V. De Pinto, F. Guarino, A. Guarnera, A. Messina, S. Reina, F.M. Tomasello, V. Palermo, C. Mazzoni, Characterization of human VDAC isoforms: a peculiar function for VDAC3? Biochim. Biophys. Acta 1797 (2010) 1268–1275, https://doi.org/10.1016/j.bbabio.2010.01.031.
[53] J. Gatliff, D. East, J. Crosby, R. Abeti, R. Harvey, W. Craigen, P. Parker, M. Campanella, TSPO interacts with VDAC1 and triggers a ROS-mediated inhibition of mitochondrial quality control, Autophagy 10 (2014) 2279–2296, https://doi.org/10.4161/15548627.2014.991665.
[54] V. Shoshan-Barmatz, A. Shteinfer-Kuzmine, A. Verma, VDAC1 at the intersection of cell metabolism, apoptosis, and diseases, Biomolecules 10 (2020) E1485, https://doi.org/10.3390/biom10111485.
[55] E.N. Maldonado, VDAC-tubulin, an anti-warburg pro-oxidant switch, Front. Oncol. 7 (2017) 4, https://doi.org/10.3389/fonc.2017.00004.
[56] M. Yang, J. Sun, D.F. Stowe, E. Tajkhorshid, W.-M. Kwok, A.K.S. Camara, Knockout of VDAC1 in H9c2 cells promotes oxidative stress-induced cell apoptosis through decreased mitochondrial hexokinase II binding and enhanced glycolytic stress, Cell. Physiol. Biochem. 54 (2020) 853–874, https://doi.org/10.33594/000000274.
[57] A.D. Chacko, F. Liberante, I. Paul, D.B. Longley, D.A. Fennell, Voltage dependent anion channel-1 regulates death receptor mediated apoptosis by enabling cleavage of caspase-8, BMC Cancer 10 (2010) 380, https://doi.org/10.1186/1471-2407-10-380.
[58] M. Poppe, C. Reimertz, H. Düßmann, A.J. Krohn, C.M. Luetjens, D. Böckelmann, A.-L. Nieminen, D. Kögel, J.H.M. Prehn, Dissipation of potassium and proton gradients inhibits mitochondrial hyperpolarization and cytochrome c release during neural apoptosis, J. Neurosci. 21 (2001) 4551–4563, https://doi.org/10.1523/JNEUROSCI.21-13-04551.2001.
[59] F. Zinghirino, X.G. Pappalardo, A. Messina, G. Nicosia, V. De Pinto, F. Guarino, VDAC genes expression and regulation in mammals, Front. Physiol. 12 (2021) 708695, https://doi.org/10.3389/fphys.2021.708695.
[60] C. Nepal, Y. Hadzhiev, P. Balwierz, E. Tarifeño-Saldivia, R. Cardenas, J.W. Wragg, A.-M. Suzuki, P. Carninci, B. Peers, B. Lenhard, J.B. Andersen, F. Müller, Dual-initiation promoters with intertwined canonical and TCT/TOP transcription start sites diversify transcript processing, Nat. Commun. 11 (2020) 168, https://doi.org/10.1038/s41467-019-13687-0.
[61] Y.J. Jang, J.H. Won, M.J. Back, Z. Fu, J.M. Jang, H.C. Ha, S. Hong, M. Chang, D. K. Kim, Paraquat induces apoptosis through a mitochondria-dependent pathway in RAW264.7 cells, Biomol Ther (Seoul) 23 (2015) 407–413, https://doi.org/10.4062/biomolther.2015.075.
[62] D.N. Criddle, S. Gillies, H.K. Baumgartner-Wilson, M. Jaffar, E.C. Chinje, S. Passmore, M. Chvanov, S. Barrow, O.V. Gerasimenko, A.V. Tepikin, R. Sutton, O. H. Petersen, Menadione-induced reactive oxygen species generation via redox cycling promotes apoptosis of murine pancreatic acinar cells, J. Biol. Chem. 281 (2006) 40485–40492, https://doi.org/10.1074/jbc.M607704200.
[63] A. Magrì, P. Risiglione, A. Caccamo, B. Formicola, M.F. Tomasello, C. Arrigoni, S. Zimbone, F. Guarino, F. Re, A. Messina, Small hexokinase 1 peptide against toxic SOD1 G93A mitochondrial accumulation in ALS rescues the ATP-related respiration, Biomedicines 9 (2021) 948, https://doi.org/10.3390/biomedicines9080948.
[64] Y. Sun, A.A. Vashisht, J. Tchieu, J.A. Wohlschlegel, L. Dreier, Voltage-dependent anion channels (VDACs) recruit Parkin to defective mitochondria to promote mitochondrial autophagy, J. Biol. Chem. 287 (2012) 40652–40660, https://doi.org/10.1074/jbc.M112.419721.
[65] H. Meyer, M. Bug, S. Bremer, Emerging functions of the VCP/p97 AAA-ATPase in the ubiquitin system, Nat. Cell Biol. 14 (2012) 117–123, https://doi.org/10.1038/ncb2407.
[66] J.-S. Ju, C.C. Weihl, Inclusion body myopathy, Paget's disease of the bone and fronto-temporal dementia: a disorder of autophagy, Hum. Mol. Genet. 19 (2010) R38–R45, https://doi.org/10.1093/hmg/ddq157.
[67] K.J. Livak, T.D. Schmittgen, Analysis of relative gene expression data using real-time quantitative PCR and the 2(-Delta Delta C(T)) Method, Methods 25 (2001) 402–408, https://doi.org/10.1006/meth.2001.1262.
[68] P.M. Quiros, A. Goyal, P. Jha, J. Auwerx, Analysis of mtDNA/nDNA ratio in mice, Curr. Protoc Mouse Biol. 7 (2017) 47–54, https://doi.org/10.1002/cpmo.21.
[69] M.F. Tomasello, F. Guarino, S. Reina, A. Messina, V.D. Pinto, The voltage-dependent anion selective channel 1 (VDAC1) topography in the mitochondrial outer membrane as detected in intact cell, PLoS One 8 (2013), e81522, https://doi.org/10.1371/journal.pone.0081522.